Wave patterns generated by a supersonic moving body in a binary Bose-Einstein condensate

Yu. G. Gladush,[1] A. M. Kamchatnov,[1] Z. Shi,[2] P. G. Kevrekidis,[2] D. J. Frantzeskakis,[3] and B. A. Malomed[4]
[1]*Institute of Spectroscopy, Russian Academy of Sciences, Troitsk, Moscow Region, 142190, Russia*
[2]*Department of Mathematics and Statistics, University of Massachusetts, Amherst Massachusetts 01003-4515, USA*
[3]*Department of Physics, University of Athens, Panepistimiopolis, Zografos, Athens 157 84, Greece*
[4]*Department of Physical Electronics, Faculty of Engineering, Tel Aviv University, Tel Aviv 69978, Israel*
(Received 13 November 2008; published 23 March 2009)

Generation of wave structures by a two-dimensional (2D) object (laser beam) moving in a 2D two-component Bose-Einstein condensate with a velocity greater than the two sound velocities of the mixture is studied by means of analytical methods and systematic simulations of the coupled Gross-Pitaevskii equations. The wave pattern features three regions separated by two Mach cones. Two branches of linear patterns similar to the so-called "ship waves" are located outside the corresponding Mach cones, and oblique dark solitons are found inside the wider cone. An analytical theory is developed for the linear patterns. A particular dark-soliton solution is also obtained, its stability is investigated, and two unstable modes of transverse perturbations are identified. It is shown that for a sufficiently large flow velocity, this instability has a convective character in the reference frame attached to the moving body, which makes the dark soliton effectively stable. The analytical findings are corroborated by numerical simulations.

DOI: 10.1103/PhysRevA.79.033623 PACS number(s): 03.75.Kk

I. INTRODUCTION

Breakdown of superfluidity at large velocities of the flow is a fundamentally important problem which has been widely studied in physics of quantum liquids, such as ^{4}He and Bose-Einstein condensates (BECs) of dilute atomic gases (see, e.g., Ref. [1] and references therein). It is known that the breakdown is caused by opening of channels for emission of elementary excitations in the fluid. This happens, in particular, with the increase of the velocity of a body ("obstacle") moving through the superfluid; in BEC experiments, a far-blue-detuned laser beam, which produces a local repulsive force acting on atoms, usually plays the role of the obstacle [2,3]. In the BEC, solitary waves and vortices are readily generated if the size of the obstacle is of the order of, or greater than, the characteristic healing length of the condensate. The formation of these structures manifests itself as an effective dissipation, which implies the loss of superfluidity at some critical value of the obstacle's velocity [4,5]. On the other hand, if the size of the obstacle is much smaller than the healing length, the main loss channel, which opens at supersonic velocities of the obstacle, corresponds to the Cherenkov emission of Bogoliubov's excitations [6,7]. If a large obstacle moves at a supersonic velocity, then the amplitude of the generated waves becomes large too. In the latter case, two dispersive shocks, which start their propagation from the front and the rear parts of the moving body, are formed. Far from the body, the front shock gradually transforms into a linear "ship wave" located outside the Mach cone [8–11], whereas the rear shock is converted into a "fan" of oblique dark solitons located inside the Mach cone [12–14]. Although, as is well known [15–17] (see also review [18]), such dark solitons are unstable with respect to transverse perturbations, it was shown in Ref. [19] that for a flow velocity greater than some critical value, this instability becomes a convective one, rather than being absolute in the reference frame moving along with the obstacle. This fact actually means that the dark solitons are effectively stable in the region around the obstacle. Some of these structures have been already observed in experiments [8,20], and similar nonstationary dispersive shocks were studied both theoretically and experimentally in BEC [2,21–24] (see also review [25]) and nonlinear optics [26–31].

The picture described above corresponds to a single-component BEC whose mean-field dynamics is governed by the respective Gross-Pitaevskii equation (GPE) [1]. At the same time, one of the focal points of activity in BEC physics has been the study of multicomponent settings, a prototypical one being presented by binary mixtures [32–34]. These two-component media exhibit phase-separation phenomena [35–37] due to the repulsion between different atomic species, or possibly different hyperfine states of the same atom, that constitute the mixture. The formation of robust single-ring and multiring patterns [33,38], the evolution of initially coincident triangular vortex lattices through a turbulent regime into an interlaced square vortex lattice [39] in coupled hyperfine states in the ^{87}Rb condensate, and the study of the interplay between atomic states at different Zeeman levels in the ^{23}Na condensate, forming striated magnetic domains in optical traps [40,41], represent some of the many possibilities that multicomponent BECs can offer. It is relevant to note that mixtures with a higher number of components, namely spinor condensates [34,42], are known too. Spinor BECs have been realized with the help of far-off-resonant optical techniques for trapping ultracold atomic gases [43], which allow the spin degree of freedom to be explored (in earlier experiments, it was frozen in magnetic traps).

Our aim in the present work is to unite these two areas by investigating effects generated by the motion of an obstacle in a "pancake"-shaped, i.e., effectively two-dimensional (2D), *two-component* BEC. In an earlier work [44], the critical situation, when the obstacle had a velocity comparable to the two speeds of sound in the two-component system, was examined. Here, we extend the analysis to the supercritical

 ©2009 The American Physical Society

case, when the speed of the moving body may be significantly higher than the sound speeds. We demonstrate that two branches of linear patterns (so-called "ship waves") form outside of the two Mach cones, which are associated with the speeds of sound, while oblique dark solitons are located inside the wider Mach cone. While these dark solitons are unstable at relatively low velocities of the motion of the obstacle, they can be *convectively stabilized* at sufficiently high values of the velocity.

The presentation is structured as follows. In Sec. II, we present the model. In Sec. III, the linear ship waves are studied by means of analytical and numerical methods. In Sec. IV, we are dealing with dark solitons again by dint of both analytical and numerical methods. The findings are summarized in Sec. V, where we also discuss potential directions for future work.

II. MODEL AND SETUP

In the mean-field approximation, the 2D flow of the binary condensate past an obstacle obeys the system of nonlinearly coupled GPEs. In the scaled form, the equations take a well-known form [1,25]

$$i\frac{\partial \psi_1}{\partial t} = -\frac{1}{2}\Delta\psi_1 + (g_{11}|\psi_1|^2 + g_{12}|\psi_2|^2)\psi_1 + V(\mathbf{r},t)\psi_1,$$

$$i\frac{\partial \psi_2}{\partial t} = -\frac{1}{2}\Delta\psi_2 + (g_{12}|\psi_1|^2 + g_{22}|\psi_2|^2)\psi_2 + V(\mathbf{r},t)\psi_2, \quad (1)$$

where Laplacian Δ acts on spatial coordinates $\mathbf{r}=(x,y)$. We assume that atoms in both species have the same mass (i.e., they represent different hyperfine states of the same atom—see, e.g., Ref. [38] and references therein) and potential $V(\mathbf{r},t)$ which represents the moving obstacle is identical for both components.

Small-amplitude waves and solitons correspond to the potential flow with zero vorticity, for which Eq. (1) can be transformed into a hydrodynamic form by means of substitutions

$$\psi_1(\mathbf{r},t) = \sqrt{n_1(\mathbf{r},t)}\exp\left[i\int^{\mathbf{r}} \mathbf{u}_1(\mathbf{r}',t)\cdot d\mathbf{r}' - i\mu_1 t\right],$$

$$\psi_2(\mathbf{r},t) = \sqrt{n_2(\mathbf{r},t)}\exp\left[i\int^{\mathbf{r}} \mathbf{u}_2(\mathbf{r}',t)\cdot d\mathbf{r}' - i\mu_2 t\right], \quad (2)$$

where $n_{1,2}(\mathbf{r},t)$ are atom densities of the two BEC components, $\mathbf{u}_{1,2}(\mathbf{r},t)$ are their velocity fields, and $\mu_{1,2}$ are the respective chemical potentials. Because the velocity field is vorticity free, the phase integrals in Eq. (2) do not depend on the integration contour, being functions of the upper limit $\mathbf{r}$ of integration only. Substituting Eq. (2) into the Eq. (1) we arrive at the following system:

$$(n_{1,2})_t + \nabla\cdot(n_{1,2}\mathbf{u}_{1,2}) = 0,$$

$$(\mathbf{u}_1)_t + (\mathbf{u}_1\cdot\nabla)\mathbf{u}_1 + g_{11}\nabla n_1 + g_{12}\nabla n_2 + \nabla\left(\frac{(\nabla n_1)^2}{8n_1^2} - \frac{\Delta n_1}{4n_1}\right) + \nabla V(\mathbf{r},t) = 0,$$

$$(\mathbf{u}_2)_t + (\mathbf{u}_2\cdot\nabla)\mathbf{u}_2 + g_{12}\nabla n_1 + g_{22}\nabla n_2 + \nabla\left(\frac{(\nabla n_2)^2}{8n_2^2} - \frac{\Delta n_2}{4n_2}\right) + \nabla V(\mathbf{r},t) = 0, \quad (3)$$

with subscript t standing for $\partial/\partial t$. The first pair of the equations represents the conservation of the number of atoms in each component, and the second pair corresponds to the Euler's equations for fluid velocities under the action of the pressure induced by interactions between atoms, the obstacle's potential, and "quantum pressure."

We consider waves generated by the obstacle moving at constant velocity U along the x axis,

$$V(\mathbf{r},t) = V(x-Ut), \quad (4)$$

through a uniform condensate so that both components have constant densities and vanishing velocities at $|x|\to\infty$. This setting implies the absence of a trapping potential in the plane of the quasi-2D BEC (or, more realistically, a very weak trapping). In the reference frame moving along with the obstacle, the unperturbed condensate flows at constant velocity $\mathbf{u}=(-U,0)$; hence the respective boundary conditions for the densities and velocities are

$$n_1 \to n_{10}, \quad n_2 \to n_{20}, \quad \mathbf{u}_1 \to \mathbf{u}, \quad \mathbf{u}_2 \to \mathbf{u} \ \text{ at } \ |x|\to\infty. \quad (5)$$

As follows from Eq. (5), chemical potentials $\mu_{1,2}$ are related to asymptotic densities n_{10}, n_{20},

$$\mu_1 = g_{11}n_{10} + g_{12}n_{20}, \quad \mu_2 = g_{12}n_{10} + g_{22}n_{20}. \quad (6)$$

In this reference frame, the wave pattern is a stationary one, which is convenient for the analysis.

III. LINEAR "SHIP WAVES"

We first consider linear waves generated by the moving obstacle, assuming that potential $V(\mathbf{r},t)$ is weak enough to allow the application of the perturbation theory based on linearized Eq. (7). Actually, the approximation is valid whenever the amplitude of the waves is small—in particular, far enough from the obstacle outside the Mach cones associated with the speeds of sound. Thus, we introduce small deviations from the uniform state,

$$n_1 = n_{10} + n_1', \quad n_2 = n_{20} + n_2', \quad \mathbf{u}_1 = \mathbf{u} + \mathbf{u}_1', \quad \mathbf{u}_2 = \mathbf{u} + \mathbf{u}_2', \quad (7)$$

and linearize Eq. (3) accordingly,

$$(n_1')_t + n_{10}(\nabla\cdot\mathbf{u}_1') + (\mathbf{u}\cdot\nabla)n_1' = 0,$$

$$(n_2')_t + n_{20}(\nabla\cdot\mathbf{u}_2') + (\mathbf{u}\cdot\nabla)n_2' = 0,$$

$$(\mathbf{u}_1')_t + (\mathbf{u}\cdot\nabla)\mathbf{u}_1' + g_{11}\nabla n_1' + g_{12}\nabla n_2' - \frac{1}{4n_{10}}\nabla(\Delta n_1') = -\nabla V, \quad (8)$$

$$(\mathbf{u}_2')_t + (\mathbf{u}\cdot\boldsymbol{\nabla})\mathbf{u}_2' + g_{12}\boldsymbol{\nabla} n_1' + g_{22}\boldsymbol{\nabla} n_2' - \frac{1}{4n_{20}}\boldsymbol{\nabla}(\Delta n_2') = -\boldsymbol{\nabla} V. \tag{9}$$

In the stationary case, all time derivatives vanish. Further, we apply the Fourier transform

$$n_1'(\mathbf{r},t) = \int\int \tilde{n}_1'(\mathbf{k},t) e^{i\mathbf{k}\cdot\mathbf{r}} \frac{d^2k}{(2\pi)^2}. \tag{10}$$

Then, we eliminate the velocity perturbations in Eq. (9) in favor of the densities, arriving at the following system of two linear equations:

$$[-(\mathbf{k}\cdot\mathbf{u})^2 + k^2(g_{11}n_{10} + k^2/4)]\tilde{n}_1' + k^2 g_{12} n_{10}\tilde{n}_2' = -k^2\tilde{V}n_{10},$$

$$k^2 g_{12} n_{20}\tilde{n}_1' + [-(\mathbf{k}\cdot\mathbf{u})^2 + k^2(g_{22}n_{20} + k^2/4)]\tilde{n}_2' = -k^2\tilde{V}n_{20}, \tag{11}$$

where tildes denote the Fourier components. This linear system can be readily solved for $\tilde{n}_{1,2}'$, and the inverse Fourier transform yields

$$n_1' = -n_{10}\int\int \frac{k^2\tilde{V}\{[-(\mathbf{k}\cdot\mathbf{u})^2 + k^2(g_{22}n_{20} + k^2/4)] - k^2 g_{12}n_{20}\}e^{i\mathbf{k}\cdot\mathbf{r}}}{[(\mathbf{k}\cdot\mathbf{u})^2 - \omega_+^2][(\mathbf{k}\cdot\mathbf{u})^2 - \omega_-^2]}\frac{d^2k}{(2\pi)^2},$$

$$n_2' = -n_{20}\int\int \frac{k^2\tilde{V}\{[-(\mathbf{k}\cdot\mathbf{u})^2 + k^2(g_{11}n_{10} + k^2/4)] - k^2 g_{12}n_{10}\}e^{i\mathbf{k}\cdot\mathbf{r}}}{[(\mathbf{k}\cdot\mathbf{u})^2 - \omega_+^2][(\mathbf{k}\cdot\mathbf{u})^2 - \omega_-^2]}\frac{d^2k}{(2\pi)^2}, \tag{12}$$

where the dispersion relations for the linear waves in the binary mixture are given by

$$\omega_\pm^2 = \tfrac{1}{2}k^2\Big[g_{11}n_{10} + g_{22}n_{20} + \tfrac{1}{2}k^2 \pm \sqrt{(g_{11}n_{10} - g_{22}n_{20})^2 + 4g_{12}^2 n_{10}n_{20}}\Big]. \tag{13}$$

In the long-wave limit, Eq. (13) yields the sound velocities [44],

$$c_\pm \equiv \lim_{k\to 0}\frac{\omega(k)}{k} = \sqrt{\frac{g_{11}n_{10} + g_{22}n_{20} \pm \sqrt{(g_{11}n_{10} - g_{22}n_{20})^2 + 4g_{12}^2 n_{10}n_{20}}}{2}}. \tag{14}$$

The presence of the two different sound velocities leads to the existence of two Mach cones defined by relations

$$\sin\theta_\pm = \frac{c_\pm}{U} \equiv \frac{1}{M_\pm}, \tag{15}$$

where $M_\pm = U/c_\pm$ are the corresponding Mach numbers and $\theta_\pm$ are angles between the direction of the obstacle's motion and the lines representing the "outer" and "inner" cones, which correspond to sound velocities c_+ and c_-, respectively. Hence, the wave pattern created by the moving obstacle is divided by the Mach cones into three regions: (i) inside the inner Mach cone, (ii) outside the outer Mach cone, (iii) and intermediate region in between the two Mach cones. The intermediate region is a feature of the two-component setting.

Expression (12) can be analyzed following the lines of Refs. [10,11]. To this end, we introduce the polar coordinates (see Fig. 1),

$$\mathbf{r} \equiv (-r\cos\chi, r\sin\chi), \quad \mathbf{k} \equiv (k\cos\eta, k\sin\eta), \tag{16}$$

and assume that the wavelength of the pattern is much greater than the characteristic size of the obstacle; hence its potential can be approximated by $V(\mathbf{r}) = V_0\delta(\mathbf{r})$. Then, we obtain

$$n_1' = \frac{4V_0 n_{10}}{\pi^2}\int_{-\pi}^{\pi}\int_0^\infty \frac{k[(g_{22} - g_{12})n_{20} + k^2/4 - U^2\cos^2\eta]e^{i\mathbf{k}\cdot\mathbf{r}}}{(k^2 - k_+^2 - i0)(k^2 - k_-^2 - i0)} \times dk\,d\eta,$$

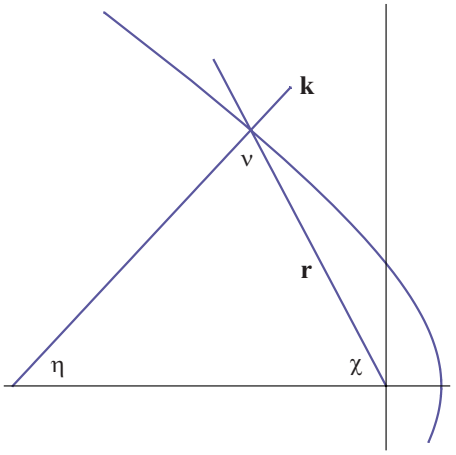

FIG. 1. (Color online) The coordinates defining radius-vector **r** and wave vector **k**. The latter one is normal to the wave front of one of the ship-wave modes, which is shown schematically by a curve.

$$n_2' = \frac{4V_0 n_{20}}{\pi^2}\int_{-\pi}^{\pi}\int_0^{\infty}\frac{k[(g_{11}-g_{12})n_{10}+k^2/4-U^2\cos^2\eta]e^{i\mathbf{k}\cdot\mathbf{r}}}{(k^2-k_+^2-i0)(k^2-k_-^2-i0)} \times dk d\eta, \tag{17}$$

where infinitesimal imaginary parts in the denominators are written to define correct contributions from the poles corresponding to adiabatically slow switching on of the potential, and

$$k_\pm \equiv 2\sqrt{U^2\cos^2\eta - c_\pm^2}. \tag{18}$$

Next, we split the integration domain of η into two parts: $\int_{-\pi/2}^{3\pi/2} d\eta \equiv \int_{-\pi/2}^{\pi/2} d\eta + \int_{\pi/2}^{3\pi/2} d\eta$. After substitution $\eta' \equiv \eta - \pi$ in the second term, one can notice that the integrand turns into its own complex conjugate, allowing one to write the integrals in Eq. (17) as

$$n_1' = \frac{8V_0 n_{10}}{\pi^2}\mathrm{Re}\int_{-\pi/2}^{\pi/2} d\eta \times \int_0^{\infty}\frac{k[(g_{22}-g_{12})n_{20}+k^2/4-U^2\cos^2\eta]e^{i\mathbf{k}\cdot\mathbf{r}}}{(k^2-k_+^2-i0)(k^2-k_-^2-i0)}dk,$$

$$n_2' = \frac{8V_0 n_{20}}{\pi^2}\mathrm{Re}\int_{-\pi/2}^{\pi/2} \times d\eta\int_0^{\infty}\frac{k[(g_{11}-g_{12})n_{10}+k^2/4-U^2\cos^2\eta]e^{i\mathbf{k}\cdot\mathbf{r}}}{(k^2-k_+^2-i0)(k^2-k_-^2-i0)}dk. \tag{19}$$

The integration over k should be carried out along the positive real half axis. However, we can add to this path a quarter of an infinite circle and the imaginary half axis in the complex k plane to build a closed integration contour. It is easy to show that the contribution from the infinite quarter circle is zero, and contribution from the imaginary axis depends on r as r^{-2}, decaying at large r much faster than the contribution from the pole, which is $\sim r^{-1/2}$. Thus, far from the obstacle, it is sufficient to keep only the contribution from the poles, which yields

$$n_1' = -\frac{2V_0 n_{10}}{\pi(c_+^2-c_-^2)}\left\{[c_+^2-(g_{22}-g_{12})n_{20}]\mathrm{Im}\int_{-\pi/2}^{\pi/2} d\eta e^{ik_+ r\cos\nu} - [c_-^2-(g_{22}-g_{12})n_{20}]\mathrm{Im}\int_{-\pi/2}^{\pi/2} d\eta e^{ik_- r\cos\nu}\right\},$$

$$n_2' = -\frac{2V_0 n_{20}}{\pi(c_+^2-c_-^2)}\left\{[c_+^2-(g_{11}-g_{12})n_{10}]\mathrm{Im}\int_{-\pi/2}^{\pi/2} d\eta e^{ik_+ r\cos\nu} - [c_-^2-(g_{11}-g_{12})n_{10}]\mathrm{Im}\int_{-\pi/2}^{\pi/2} d\eta e^{ik_- r\cos\nu}\right\}, \tag{20}$$

where $\nu \equiv \pi - \chi - \eta$. Far from the obstacle, where phases $\mathbf{k}_\pm\mathbf{r} = rs_\pm$ with

$$s_\pm(\eta) = k_\pm(\eta)\cos(\chi+\eta) \tag{21}$$

are large, the integrals in Eq. (20) can be estimated by means of the stationary-phase method. Since calculations of both integrals are identical, we consider for definiteness, the integration over k_+. Condition $\partial s_+/\partial\eta = 0$ determines the stationary-phase point, which can be easily cast in the form of

$$\tan(\nu_+) = (2U^2/k_+^2)\sin(2\eta_+). \tag{22}$$

Taking into regard the definition of ν, we obtain from here an expression for χ,

$$\tan(\chi_+) = \frac{[1+k_+^2/(2c_+^2)]\tan(\eta_+)}{U^2/c_+^2 - [1+k_+^2/(2c_+^2)]}, \tag{23}$$

with η_+ taking values in interval

$$-\arccos\left(\frac{1}{M_+}\right) \le \eta_+ \le \arccos\left(\frac{1}{M_+}\right), \quad M_+ \equiv \frac{U}{c_+}, \tag{24}$$

while the corresponding vector $\{x,y\}$, given by the parametric expressions,

$$x(\eta_+) = \frac{4\phi c_+^2}{k_+^3}[M_+^2\cos(2\eta_+)-1]\cos(\eta_+),$$
$$y(\eta_+) = \frac{4\phi c_+^2}{k_+^3}[2M_+^2\cos^2(\eta_+)-1]\sin(\eta_+), \tag{25}$$

moves along a curve with constant phase ϕ (e.g., a crest line).

As usual in the method of stationary phase, we reduce the integrals in Eq. (20) to Gaussian ones, which yields a final result,

$$n_1' = -\frac{2V_0 n_{10}}{\pi(c_+^2-c_-^2)}\left\{[c_+^2-(g_{22}-g_{12})n_{20}]\sqrt{\frac{2\pi}{k_+ r}}\frac{[1+(4U^2/k_+^2)\sin^2(2\eta_+)]^{1/4}}{[1+(4U^2/k_+^2)\cos(2\eta_+)+(12U^4/k_+^4)\sin^2(2\eta_+)]^{1/2}}\cos(k_+ r\cos\nu_+ - \pi/4) - [c_-^2-(g_{22}-g_{12})n_{20}]\sqrt{\frac{2\pi}{k_- r}}\frac{[1+(4U^2/k_-^2)\sin^2(2\eta_-)]^{1/4}}{[1+(4U^2/k_-^2)\cos(2\eta_-)+(12U^4/k_-^4)\sin^2(2\eta_-)]^{1/2}}\times\cos(k_- r\cos\nu_- - \pi/4)\right\}, \tag{26}$$

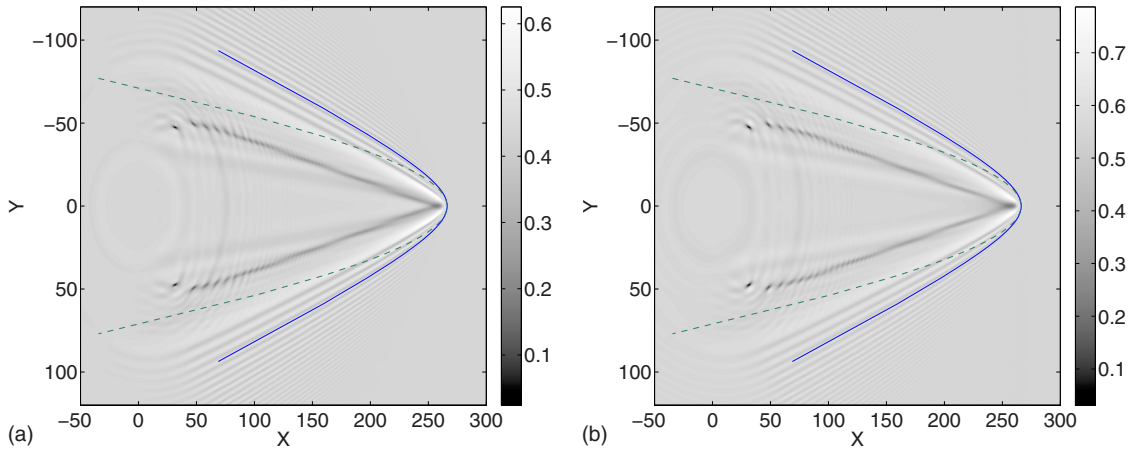

FIG. 2. (Color online) Spatial contour plots of densities of the two components (left and right panels, respectively) in the binary BEC for flow velocity $U=3.5$, at $t=75$. The form of the obstacle's potential used in this case is $V(x,y,t)=2\ \mathrm{sech}^2(\sqrt{(x-Ut)^2+y^2}/2)$. Solid and dashed thin lines correspond to wave crests of two modes of the ship waves.

where $\nu_\pm \equiv \pi-\chi_\pm-\eta_\pm$ and similar expressions can be derived for the density oscillations of the second component of the binary condensate.

An example of wave patterns generated by numerical simulations of Eq. (1) is displayed in Fig. 2 for parameters $g_{11}=1.5$, $g_{22}=1.25$, $g_{12}=1.0$, $n_{10}=1.0$, $n_{20}=2.0$, and velocity $U=3.5$.

Three different types of waves can clearly be distinguished in this picture. First, one observes ship waves outside the Mach cones, which were analyzed above (the mode between the two cones has a smaller amplitude than the mode outside the outer Mach cone for chosen values of the parameters). Second, oblique dark solitons are observed inside the outer Mach cone; they will be discussed in Sec. IV. Also, third, one can also notice that oblique solitons and ship waves located between the Mach cones are modulated by concentric circular waves, which were actually generated by the initial switching on of the obstacle's potential. These circular waves are not related to the steady regime and are not considered hereafter.

We have compared the analytical results of Eq. (25) for the crest lines with the numerical findings. The analytically predicted curves are shown by thin solid and dashed lines in Fig. 2 and they demonstrate good agreement with numerical simulations. It is worth noticing that the ship waves between the Mach cones interact elastically with the oblique solitons. As a result, the solitons are slightly broken at points where they are crossed by the crest lines of the ship waves. Besides that, the oblique solitons are modulated by the cylindrical waves produced by the initial pulse, as mentioned above. If parameters of the binary BEC are chosen so as to make the chemical potentials [Eq. (6)] of both components equal, then the smaller sound velocity is given by $c_-^2=(g_{11}-g_{12})n_{10}=(g_{22}-g_{12})n_{20}$; hence the last term in Eq. (26), as well as in the similar expression for n_2, vanishes, and the ship waves in the region between the two Mach cones are not visible in this case. We have also checked this prediction and concluded that the mode between two Mach cones indeed completely disappears at $\mu_1=\mu_2$.

Amplitudes of the ship waves are predicted by Eq. (26) only qualitatively, as these expressions correspond to the far-field region, whereas in numerical simulations only a near-field region can be simulated effectively enough. Nevertheless, the analytical predictions provide correct estimates for the amplitude and its coordinate dependence.

IV. OBLIQUE DARK SOLITONS

As mentioned above, in Fig. 2 one can observe oblique dark solitons located inside the outer Mach cone. It is worthy to note that they decay into vortices at end points, which is a result of the "snaking" instability of dark-soliton stripes in the 2D geometry [15–17] (see also review [18]). However, for large velocities U this instability is convective only [19], which means that the dark solitons may be effectively stable around the obstacle and, hence, the length of the dark-solitons' crests increases with time. The solitons originate from a depression in the density distribution formed behind the obstacle by the flow, therefore their depth also varies near the obstacle. However, upon sufficiently long evolution time, there exists a region where the oblique dark solitons can be considered as quasistationary structures. In this region, the solitons are described by the stationary solution of the GPEs. This allows us to take the stationary GPEs in the hydrodynamic form of Eq. (3),

$$\nabla\cdot(n_{1,2}\mathbf{u}_{1,2})=0,$$

$$(\mathbf{u}_1\cdot\nabla)\mathbf{u}_1+g_{11}\nabla n_1+g_{12}\nabla n_2+\nabla\left[\frac{(\nabla n_1)^2}{8n_1^2}-\frac{\Delta n_1}{4n_1}\right]=0,$$

$$(\mathbf{u}_2\cdot\nabla)\mathbf{u}_2+g_{12}\nabla n_1+g_{22}\nabla n_2+\nabla\left[\frac{(\nabla n_2)^2}{8n_2^2}-\frac{\Delta n_2}{4n_2}\right]=0. \tag{27}$$

Here, it is taken into regard that the obstacle's potential is negligible far from it. Equation (27) should be solved with boundary conditions

$$n_1 \to n_{10}, \quad n_2 \to n_{20}, \quad \mathbf{u}_1 \to (-U,0),$$
$$\mathbf{u}_2 \to (-U,0) \ \text{ at } \ |x| \to \infty, \tag{28}$$

where $-U$ is the common velocity of both components relative to the obstacle. Under the assumption that the solution depends only on

$$\xi = \frac{x-ay}{\sqrt{1+a^2}}, \tag{29}$$

where a determines the slope of the oblique dark soliton, this system can be readily reduced to the following equations (with the prime standing for $d/d\xi$):

$$(1/8)[(n_1')^2 - 2n_1 n_1''] + g_{11}n_1^3 + g_{12}n_1^2 n_2 + \frac{1}{2}qn_{10}^2 - \left(\frac{1}{2}q+\mu_1\right)n_1^2 = 0,$$

$$(1/8)[(n_2')^2 - 2n_2 n_2''] + g_{12}n_1 n_2^2 + g_{22}n_2^3 + \frac{1}{2}qn_{20}^2 - \left(\frac{1}{2}q+\mu_2\right)n_2^2 = 0, \tag{30}$$

where μ_1 and μ_2 are the chemical potentials defined above in Eq. (6) and

$$q \equiv \frac{U^2}{1+a^2}. \tag{31}$$

The flow velocities are related to the densities as follows:

$$\mathbf{u}_i = \left\{ \frac{(n_{i0}+a^2 n_i)U}{(1+a^2)n_i}, \quad -\frac{aU(n_{i0}-n_i)}{(1+a^2)n_i} \right\}, \quad i=1,2. \tag{32}$$

In general, system (30) has to be solved numerically. However, if the chemical potentials of the two components are again taken to be equal,

$$\mu_1 = \mu_2 = \mu, \tag{33}$$

the system admits a simple analytical solution. In this case, we look for the solution as $n_1 = n_{10}f(\xi)$, $n_2 = n_{20}f(\xi)$, reducing both Eq. (30) to a single one,

$$\frac{1}{8}[(f')^2 - 2ff''] + \mu f^3 + \frac{1}{2}q - \left(\frac{1}{2}q+\mu\right)f^2 = 0. \tag{34}$$

Dark-soliton solutions to Eq. (34) are known [13],

$$n_1 = n_{1s} = n_{10}f(\xi), \quad n_2 = n_{2s} = n_{20}f(\xi), \quad f(\xi) = 1 - \frac{1-q/c_+^2}{\cosh^2[\sqrt{c_+^2-q}(x-ay)/\sqrt{1+a^2}]}, \tag{35}$$

where we have taken into regard that condition (33) leads to the following expressions for the sound velocities (for the definiteness, we suppose here that $g_{11}, g_{22} > g_{12}$, i.e., the interspecies repulsion is weaker than the repulsive self-interactions of the two components):

$$c_-^2 = (g_{11}-g_{12})n_{10}, \quad c_+^2 = \mu. \tag{36}$$

Obviously, solution (35) exists if condition $q < c_+^2$ is satisfied. If we introduce the angle θ between the direction of the flow and the orientation of the dark-soliton stripe, so that $a = \cot\theta$, the latter condition can be transformed into

$$\sin^2\theta < \frac{c_+^2}{U^2} = \frac{1}{M_+^2}, \quad M_+ \equiv \frac{U}{c_+}. \tag{37}$$

Thus, the soliton must be located inside the outer Mach cone, which is defined by the Eq. (15). Although we have arrived at this conclusion under assumption (33), we conjecture that it is correct too in the general case of unequal chemical potentials, which is confirmed by our numerical simulations, that always produced oblique solitons confined inside the outer Mach cone. The respective numerically generated profiles of the densities are shown in Fig. 3 as a function of y at a fixed value of x; the corresponding phase profiles are also shown in the figure. It is observed that the oblique solitons are indeed located inside the outer Mach cone [as defined by Eq. (37)]) but outside of the inner cone, which is defined by $\sin(\theta_-) = 1/M_-$. Profiles of the solitons' densities are close to the analytically predicted ones, and the phase jumps are also in agreement with the expected dark-soliton behavior.

According to condition (37), solution (35) exists for any supersonic flow with $U > c_+$, the same being true for the existence of numerical solutions to system (30) in the general case, $\mu_1 \neq \mu_2$. However, that does not mean that the oblique dark solitons can be generated by any such flow. While the numerical results presented in Fig. 2 show that oblique solitons indeed exist for velocity $U=3.5$, another situation, when oblique dark solitons do not emerge, is presented in Fig. 4 by means of density patterns which correspond to a lower supersonic flow velocity, $U=1.2$. In the latter case, it is observed that vortex streets are generated, rather than dark solitons. Such a behavior is related to the above-mentioned instability of dark solitons with respect to transverse perturbations [15–17]. The instability splits dark solitons into vortex-antivortex pairs; hence dark solitons cannot develop from the density depression behind the obstacle moving at a relatively low velocity. However, the numerical simulations presented in Fig. 2 indicate that the oblique solitons become effectively stable if the flow velocity is sufficiently high, as first was noticed in Ref. [13] for the case of the one-component BEC. As said above, the stabilization was explained in Ref. [19] as the transition from the absolute instability of dark solitons to their convective instability, at some critical value of the flow velocity, $U_{cr} \geq c_+$. In that case, unstable disturbances are carried away by the flow from the region around the obstacle, where, as a result, the dark solitons look as effectively stable objects. Here, we aim to consider such a stabilization transition for the case of the two-component BEC, which features two unstable modes of perturbations around dark solitons.

To find the spectrum of small-amplitude linear waves propagating along the dark soliton, we now consider this solution in the reference frame in which the condensate has zero velocity far from the obstacle. To this end, we rotate the coordinate system by angle $\varphi = \arctan a$ [recall that the angle

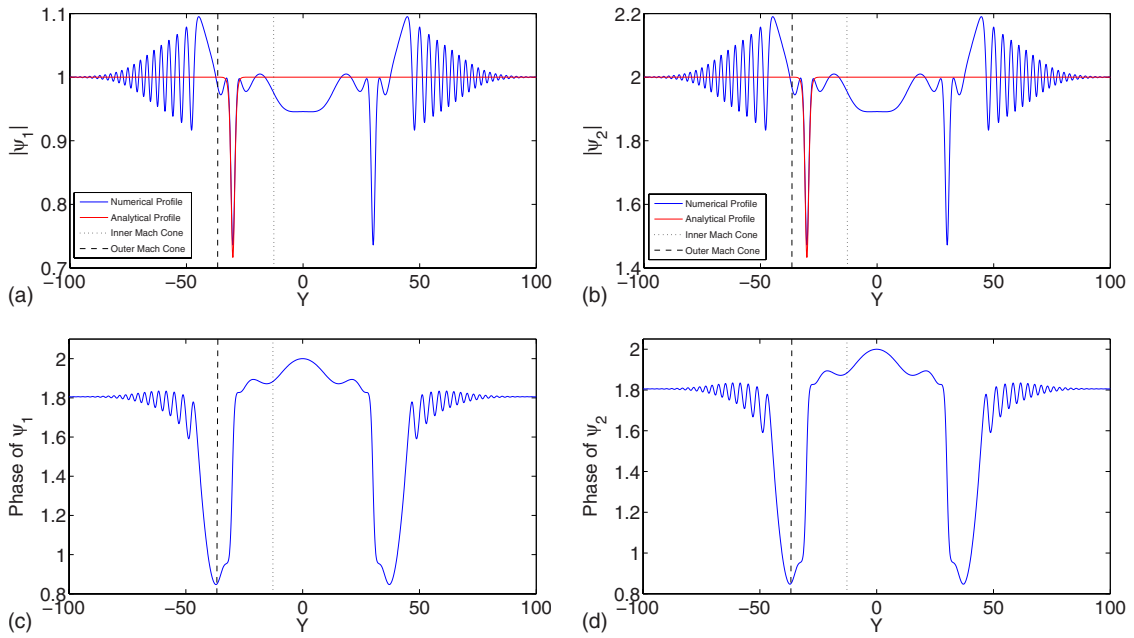

FIG. 3. (Color online) Plots of densities (top) and phases (bottom) of the two BEC components for flow velocity $U=4.5$. The positions of the Mach cones are shown by dashed lines, making it evident that the oblique dark solitons are located inside the outer Mach cone, in agreement with Eq. (37). The chemical potentials are $\mu_1=\mu_2=3.5$, cf. Eq. (33), and the configurations are shown at $t=30$. The phases of both components coincide with each other in the case of equal chemical potentials, and the densities have the same profile multiplied by the density at infinity.

a determines the orientation of the dark soliton, according to Eq. (29)], and perform the Galilean transformation to the frame moving relative to the obstacle at velocity $(U\cos\varphi, U\sin\varphi)$,

$$\tilde{x} = x\cos\varphi - y\sin\varphi - U\cos\varphi t,$$

$$\tilde{y} = x\sin\varphi + y\cos\varphi - U\sin\varphi t. \tag{38}$$

After the transformation, the velocity fields (32) become

$$\tilde{\mathbf{u}}_1 = (v(n_{10}/n_{1s}-1),0), \quad \tilde{\mathbf{u}}_2 = (v(n_{20}/n_{2s}-1),0), \tag{39}$$

and the densities take the form of

$$\tilde{n}_{1s} = n_{10}f(\zeta), \quad \tilde{n}_{2s} = n_{20}f(\zeta),$$

$$f(\zeta) = 1 - \frac{1-(v^2/c_+^2)}{\cosh^2[\sqrt{c_+^2-v^2}\zeta]}, \quad \zeta = \tilde{x} - vt, \tag{40}$$

where the soliton's velocity in the new reference frame is

$$v = \frac{U}{\sqrt{1+a^2}}. \tag{41}$$

Below, we omit tildes attached to the new variables.

We take small transverse perturbations around the dark-soliton solution as

$$\psi_1 = \psi_{1s}(\zeta) + (\psi_1 + i\psi_1'')\exp[i\phi_{1s}(\zeta) - i\mu_1 t],$$

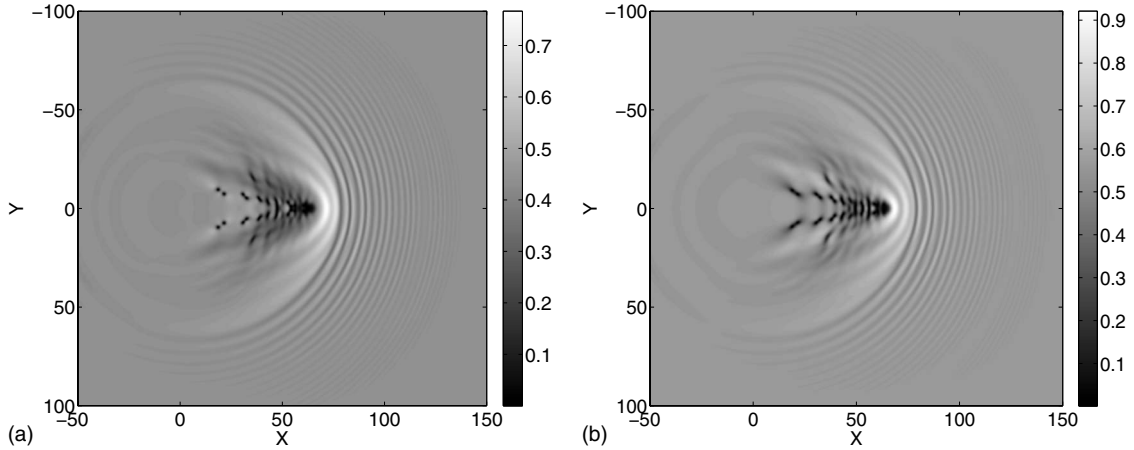

FIG. 4. Plots of densities of two BEC components for flow velocity $U=1.2$ at $t=55$. In this case, oblique dark solitons do not emerge.

$$\psi_2 = \psi_{2s}(\zeta) + (\psi_2 + i\psi_2'')\exp[i\phi_{2s}(\zeta) - i\mu_2 t], \tag{42}$$

where the unperturbed solution depends only on $\zeta = x - vt$,

$$\psi_{js} = \sqrt{n_{js}}\,\exp[i\phi_{js}(\zeta) - i\mu_j t], \tag{43}$$

and phases ϕ_{js} are related to the densities by equations

$$\frac{\partial \phi_{js}}{\partial \zeta} = v\left(\frac{n_{j0}}{n_{js}} - 1\right). \tag{44}$$

Perturbations ψ' and $i\psi''$ depend on y and t as $\exp(ipy + \Gamma t)$. The substitution of expressions (42) into Eq. (1) and linearization with respect to ψ' and $i\psi''$ lead to the following eigenvalue problem:

$$\begin{pmatrix} A_1 & -L_{I1} & 0 & 0 \\ L_{R1} & A_1 & B & 0 \\ 0 & 0 & A_2 & -L_{I2} \\ B & 0 & L_{R2} & A_2 \end{pmatrix} \begin{pmatrix} \psi_1' \\ \psi_1'' \\ \psi_2' \\ \psi_2'' \end{pmatrix} = \Gamma \begin{pmatrix} \psi_1' \\ \psi_1'' \\ \psi_2' \\ \psi_2'' \end{pmatrix}, \tag{45}$$

$$A_j \equiv \frac{v n_{j0} n_{js,\zeta}}{2 n_{js}^2} - \frac{v n_{j0}}{n_{js}} \frac{\partial}{\partial \zeta},$$

$$B \equiv -2 g_{12} \sqrt{n_{1s} n_{2s}},$$

$$L_{Ij} \equiv \frac{1}{2}\frac{\partial^2}{\partial \zeta^2} - \frac{1}{2}\frac{n_{j0}^2 v^2}{n_{js}^2} + \frac{1}{2}(v^2 - p^2) - g_{jj} n_{js} - g_{lj} n_{ls} + \mu_j, \tag{46}$$

$$L_{Rj} \equiv \frac{1}{2}\frac{\partial^2}{\partial \zeta^2} - \frac{1}{2}\frac{n_{j0}^2 v^2}{n_{js}^2} + \frac{1}{2}(v^2 - p^2) - 3 g_{jj} n_{js} - g_{lj} n_{ls} + \mu_j,$$

$$j = 1,2, \quad l = 1,2, \quad l \neq j.$$

System (45) determines growth rates $\Gamma_{1,2}(p)$ of small perturbations traveling along the dark-soliton's crest. As a result, two unstable branches have been found, examples of which are shown in Fig. 5. One can see that both branches feature regions of wave vector p with $\mathrm{Re}\,\Gamma(p) > 0$. The transition to the convective instability should be considered separately for each branch.

Returning to the reference system attached to the moving obstacle, we arrive at dispersion relations

$$\omega_{1,2}(p) = U_s p + i\Gamma(p, v), \tag{47}$$

where $U_s = v \sin\varphi \equiv aU/\sqrt{1+a^2}$ is the component of the flow velocity along the dark soliton. The perturbations may be represented as Fourier integrals over linear modes obeying dispersion relations (47),

$$\delta n_{1,2} \propto \int_{-\infty}^{\infty} \delta\tilde{n}_{1,2}(p) e^{i[py - \omega_{1,2}(p)t]} dp. \tag{48}$$

This representation implies that the integral is convergent, i.e., the wave packet is finite along coordinate y. Its time dependence at fixed value of y is determined by dispersion relations $\omega_{1,2}(p)$. Since expressions (47) contain imaginary parts, $\delta n_{1,2}$ can grow exponentially in time, which implies instability of the dark soliton, as is well known for the zero flow, $U_s = 0$. However, it may happen that, for U_s large enough, wave packets are carried away so fast that they cannot grow at fixed value of y, which is precisely the transition from absolute to convective instability [45]. Mathematically, the convective instability means that one can transform integrals over p in wave packets (48) into integrals over ω because these wave packets have finite duration. In other words, the function $\omega = \omega(p)$ can be inverted to define a single-valued dependence, $p = p(\omega)$. Thus, the distinction between the absolute and convective instabilities depends on analytical properties of dispersion relations (47) [45,46]. Actually, the transition from absolute to convective instability is determined by critical points p_{cr}, at which the derivative vanishes, $d\omega/dp = 0$, and the function $p = p(\omega)$ changes its behavior: at $U_s < (U_s)_{\mathrm{cr}}$ it is represented in the complex-p plane by disconnected curves, whereas for $U_s > (U_s)_{\mathrm{cr}}$ these curves are connected with each other. In the latter case, one can deform the contour of the integration over p, with regard to the single-valuedness of $\omega = \omega(p)$, allowing to transform it, as said above, into an integral over ω. In other words, the spatial Fourier decomposition of the perturbation wave packet can be transformed into a temporal form, which actually means that the instability is convective.

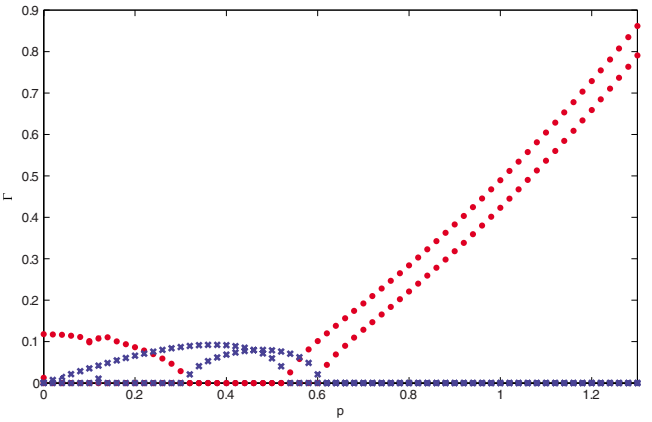

FIG. 5. (Color online) Two branches of dispersion curves $\Gamma(p)$ for unstable disturbances around the dark-soliton solution. Real parts of Γ are shown by crosses, and imaginary parts by dots. Parameters are $g_{11} = 1$, $g_{22} = 1.6$, $g_{12} = 0.1$, $n_{10} = 1$, and $n_{20} = 0.6$.

As is known, the asymptotic behavior of integrals (48) is determined by branching points of the function $p = p(\omega)$, where $d\omega/dp = 0$. This yields equation

$$U_s = -i\frac{d\Gamma}{dp}, \tag{49}$$

where, as one can see in Fig. 5, $\Gamma(p, v)$ has either real or purely imaginary values for real p. Therefore, critical values of U_s, at which disconnected contours transform into connected ones, correspond to the appearance of a double root p_{br} of Eq. (49) on the real axis of p. This means $dp_{\mathrm{br}}/dU_s \to \infty$ at $U_s = (U_s)_{\mathrm{cr}}$. Then, the differentiation of Eq. (49) with respect to U_s leads to equation

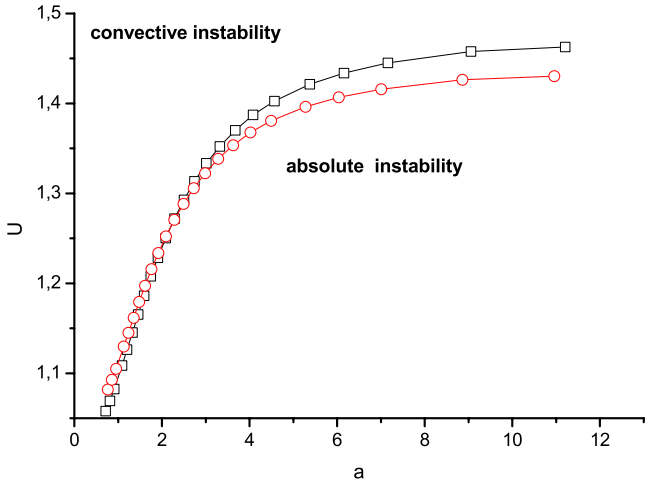

FIG. 6. (Color online) Curves separating regions of the absolute and convective instabilities of dark solitons in the two-component condensate with parameters $g_{11}=1$, $g_{22}=1.6$, $g_{12}=0.1$, $n_{10}=1$, and $n_{20}=0.6$. The respective sound velocities are $c_+=1.03, c_-=0.95$. Squares and circles refer to two different unstable modes. Below each curve, the corresponding mode is absolutely unstable and dark solitons cannot be created by the flow with velocity U less than $U_{\rm cr}\cong 1.5$, for most values of slope a. Dark solitons become convectively unstable (i.e., effectively stable) above both curves, i.e., for $U>u_{\rm cr}\cong 1.5$.

$$\left.\frac{d^2\Gamma}{dp^2}\right|_{p=p_{\rm cr}}=0 \tag{50}$$

for the corresponding critical value, $p_{\rm cr}(v)$. The substitution of that value into Eq. (49) yields function $U_s(v)$. When this function is known, we find, with the help of relations

$$v=\frac{U}{\sqrt{1+a^2}},\quad U_s=U\sin\varphi=\frac{Ua}{\sqrt{1+a^2}}=av, \tag{51}$$

the slope and velocity,

$$a_{\rm cr}(v)=\frac{U_s(v)}{v}, \tag{52}$$

$$U(v)=v\sqrt{1+a_{\rm cr}^2(v)}, \tag{53}$$

as functions of v for all values in interval $(0<v<c_+)$. As a result, we obtain, in a parametric form, the dependence $U(a)$ for the curve separating regions of the absolute and convective instabilities. Two such curves for both branches are shown in Fig. 6, where the region of the convective instability is located above the curves.

It is seen that the dark solitons with large slope a undergo the transition to the convective instability at flow velocities greater than $U_{\rm cr}\approx 1.5$, as suggested also by the numerical findings reported above.

V. CONCLUSION

We have considered the effect of the supercritical motion of a small obstacle through a two-component Bose-Einstein condensate. Our study was motivated by a number of recent experiments in such settings, which examine the dynamics of mixtures of hyperfine states of ^{87}Rb. The presence of two speeds of sound in the mixture results in the existence of two Mach cones. The motion of the obstacle, in turn, produces two main features, namely, the linear "ship waves" and oblique dark solitons. For the former pattern, we have developed a description of their density oscillations, which occur outside the Mach cones, in good agreement with numerical findings. On the other hand, for the dark solitons we have developed an analytical description of their profile, which was also found to be in good agreement with numerical observations. In particular, it was predicted that the dark solitons are confined to the area inside the outer Mach cone, which was confirmed by the simulations.

This work may be a relevant starting point toward a more detailed understanding of the interplay between interspecies interactions and the loss of superfluidity caused by the supercritical motion of defects. A natural extension of the present setting may be the consideration of the three-dimensional context, with *vortex rings* being formed as a result of the motion of the obstacle, which is closest to the experimental settings reported in Refs. [2,3]. Another possibility would be to consider the supercritical motion of the obstacle in a multicomponent spinor BEC, where it would be relevant to examine the role of the spin-dependent and spin-independent parts of the interatomic interactions (see, e.g., discussion in recent work [47]) in producing patterns such as those considered herein. Such studies are currently in progress and will be reported in future works.

ACKNOWLEDGMENTS

We appreciate a valuable discussion with L. P. Pitaevskii. Y.G.G. and A.M.K. thank RFFI (Russia) for financial support. P.G.K. gratefully acknowledges support from NSF under Contracts No. NSF-CAREER, No. NSF-DMS-0619492, and No. NSF-DMS-0806762, as well as from the Alexander von Humboldt Foundation. The work of D.J.F. was partially supported by the Special Research Account of the University of Athens. B.A.M. appreciates a partial support provided by the German-Israel Foundation through Grant No. 149/2006.

[1] L. P. Pitaevskii and S. Stringari, *Bose-Einstein Condensation* (Cambridge University Press, Cambridge, 2003).
[2] P. Engels and C. Atherton, Phys. Rev. Lett. **99**, 160405 (2007).
[3] J. J. Chang, P. Engels, and M. A. Hoefer, Phys. Rev. Lett. **101**, 170404 (2008).
[4] V. Hakim, Phys. Rev. E **55**, 2835 (1997).
[5] R. Carretero-González, P. G. Kevrekidis, D. J. Frantzeskakis, B. A. Malomed, S. Nandi, and A. R. Bishop, Math. Comput.

Simul. **74**, 361 (2007).
[6] D. L. Kovrizhin and L. A. Maksimov, Phys. Lett. A **282**, 421 (2001).
[7] G. E. Astrakharchik and L. P. Pitaevskii, Phys. Rev. A **70**, 013608 (2004).
[8] I. Carusotto, S. X. Hu, L. A. Collins, and A. Smerzi, Phys. Rev. Lett. **97**, 260403 (2006).
[9] Yu. G. Gladush, G. A. El, A. Gammal, and A. M. Kamchatnov, Phys. Rev. A **75**, 033619 (2007).
[10] Yu. G. Gladush and A. M. Kamchatnov, Zh. Eksp. Teor. Fiz. **132**, 589 (2007) [JETP **105**, 520 (2007)].
[11] Yu. G. Gladush, L. A. Smirnov, and A. M. Kamchatnov, J. Phys. B **41**, 165301 (2008).
[12] G. A. El and A. M. Kamchatnov, Phys. Lett A **350**, 192 (2006); **352**, 554(E) (2006).
[13] G. A. El, A. Gammal, and A. M. Kamchatnov, Phys. Rev. Lett. **97**, 180405 (2006).
[14] G. A. El, Yu. G. Gladush, and A. M. Kamchatnov, J. Phys. A: Math. Theor. **40**, 611 (2007).
[15] B. B. Kadomtsev and V. I. Petviashvili, Sov. Phys. Dokl. **15**, 539 (1970).
[16] V. E. Zakharov, JETP Lett. **22**, 172 (1975).
[17] E. A. Kuznetsov and S. K. Turitsyn, Sov. Phys. JETP **67**, 1583 (1988).
[18] P. G. Kevrekidis and D. J. Frantzeskakis, Mod. Phys. Lett. B **18**, 173 (2004).
[19] A. M. Kamchatnov and L. P. Pitaevskii, Phys. Rev. Lett. **100**, 160402 (2008).
[20] E. A. Cornell, Conference on Nonlinear Waves, Integrable Systems and their Applications, Colorado Springs, 2005 (unpublished) (http://jilawww.colorado.edu/bec/papers.html).
[21] B. Damski, Phys. Rev. A **69**, 043610 (2004).
[22] A. M. Kamchatnov, A. Gammal, and R. A. Kraenkel, Phys. Rev. A **69**, 063605 (2004).
[23] T. P. Simula, P. Engels, I. Coddington, V. Schweikhard, E. A. Cornell, and R. J. Ballagh, Phys. Rev. Lett. **94**, 080404 (2005).
[24] M. A. Hoefer, M. J. Ablowitz, I. Coddington, E. A. Cornell, P. Engels, and V. Schweikhard, Phys. Rev. A **74**, 023623 (2006).
[25] R. Carretero-González, D. J. Frantzeskakis, and P. G. Kevrekidis, Nonlinearity **21**, R139 (2008).
[26] W. Wan, S. Jia, and J. W. Fleischer, Nat. Phys. **3**, 46 (2007).
[27] N. Ghofraniha, C. Conti, G. Ruocco, and S. Trillo, Phys. Rev. Lett. **99**, 043903 (2007).
[28] C. Barsi, W. Wan, C. Sun, and J. W. Fleischer, Opt. Lett. **32**, 2930 (2007).
[29] S. Jia, W. Wan, and J. W. Fleischer, Phys. Rev. Lett. **99**, 223901 (2007).
[30] G. A. El, A. Gammal, E. G. Khamis, R. A. Kraenkel, and A. M. Kamchatnov, Phys. Rev. A **76**, 053813 (2007).
[31] E. G. Khamis, A. Gammal, G. A. El, Yu. G. Gladush, and A. M. Kamchatnov, Phys. Rev. A **78**, 013829 (2008).
[32] C. J. Myatt, E. A. Burt, R. W. Ghrist, E. A. Cornell, and C. E. Wieman, Phys. Rev. Lett. **78**, 586 (1997).
[33] D. S. Hall, M. R. Matthews, J. R. Ensher, C. E. Wieman, and E. A. Cornell, Phys. Rev. Lett. **81**, 1539 (1998).
[34] D. M. Stamper-Kurn, M. R. Andrews, A. P. Chikkatur, S. Inouye, H.-J. Miesner, J. Stenger, and W. Ketterle, Phys. Rev. Lett. **80**, 2027 (1998).
[35] M. Trippenbach, K. Goral, K. Rzazewski, B. Malomed, and Y. B. Band, J. Phys. B **33**, 4017 (2000).
[36] I. M. Merhasin, B. A. Malomed, and R. Driben, J. Phys. B **38**, 877 (2005).
[37] K. Kasamatsu and M. Tsubota, Phys. Rev. A **74**, 013617 (2006).
[38] K. M. Mertes, J. W. Merrill, R. Carretero-González, D. J. Frantzeskakis, P. G. Kevrekidis, and D. S. Hall, Phys. Rev. Lett. **99**, 190402 (2007).
[39] V. Schweikhard, I. Coddington, P. Engels, S. Tung, and E. A. Cornell, Phys. Rev. Lett. **93**, 210403 (2004).
[40] H.-J. Miesner, D. M. Stamper-Kurn, J. Stenger, S. Inouye, A. P. Chikkatur, and W. Ketterle, Phys. Rev. Lett. **82**, 2228 (1999).
[41] J. Stenger, S. Inouye, D. M. Stamper-Kurn, H.-J. Miesner, A. P. Chikkatur, and W. Ketterle, Nature (London) **396**, 345 (1999).
[42] M.-S. Chang, C. D. Hamley, M. D. Barrett, J. A. Sauer, K. M. Fortier, W. Zhang, L. You, and M. S. Chapman, Phys. Rev. Lett. **92**, 140403 (2004).
[43] D. M. Stamper-Kurn and W. Ketterle, in *Coherent Atomic Matter Waves, Les Houches Summer School Session LXXII in 1999*, edited by R. Kaiser, C. Westbrook, and F. David (Springer, New York, 2001), pp. 137–217.
[44] H. Susanto, P. G. Kevrekidis, R. Carretero-González, B. A. Malomed, D. J. Frantzeskakis, and A. R. Bishop, Phys. Rev. A **75**, 055601 (2007).
[45] E. M. Lifshitz and L. P. Pitaevskii, *Physical Kinetics* (Pergamon, London, 1981).
[46] P. A. Sturrock, Phys. Rev. **112**, 1488 (1958).
[47] B. J. Dabrowska-Wüster, E. A. Ostrovskaya, T. J. Alexander, and Yu. S. Kivshar, Phys. Rev. A **75**, 023617 (2007).